Preprints of the 19th World Congress
The International Federation of Automatic Control
Cape Town, South Africa. August 24-29, 2014

Effect of detector blurring on apical region in myocardial perfusion SPECT imaging

Gábor Hesz * **Béla Kári** *** **Ákos Szlávecz** * **András Wirth** **
Oszkár Pártos **** **Balázs Benyó** *

* *Department of Control Engineering and Information Technology, Budapest University of Technology and Economics, H-1117 Budapest, Magyar tudósok körútja 2.*
** *Mediso Ltd., H-1022 Budapest, Alsótörökvész 14., Hungary*
*** *Semmelweis University, Department of Radiology and Oncotherapy/Department of Nuclear Medicine, H-1082 Üllöi út 78/a*
**** *Semmelweis University, Department of Nuclear Medicine, H-1082 Üllöi út 78/a*

Abstract: One of the largest application fields of the Single Photon Emission Computed Tomography (SPECT) technology is parallel imaging based myocardial perfusion scintigraphy. Any image improvements resulting from the evaluation of the distortions and noise phenomena have significant diagnostic value in this field. Several distortion effects have been compensated inherently - non-uniform photon abortion and non-linear distant dependent spatial resolution (DDSR) effects of the imaging - by our developed novel 3D iterative reconstruction method. However, equivocal hypo-perfusion segment have been detected around the apical region of the myocardium systematically on both mathematical phantoms, physical phantoms, and in human studies. We concluded that the Partial Volume Effect (PVE) phenomenon may cause the distortion. The aim of the current research is to discover the impact of the 3D parallel projection based reconstruction parameters on the apical lesion effect.
Several reconstruction setups with different parameter settings are executed using different mathematical phantoms to model the myocardium. The reconstructed images are compared with quantitative measures. The degree of apical lesion is decreased if a volume of 256^3 with voxel sizes of $2mm$ was applied instead of a volume of 128^3 with voxel sizes of $4mm$. Higher resolution volumes caused reduced Partial Volume Effect. In addition, a lesser extent of detector blurring resulted in less apical lesion. Further investigations are planned to analyze relationship between reconstruction setups and apical lesion.

Keywords: Medical Imaging, Nuclear Medicine, SPECT, Image Reconstruction, Myocardial Perfusion Imaging, Apical Lesion

1. INTRODUCTION

Single Photon Emission Computed Tomography (SPECT) (Miles N. Wernick (2005)) is a widely used nuclear imaging technique. During SPECT imaging a radiolabeled substance is injected into the patient to examine a biological function or a function of organ. 2D projections of the 3D activity distribution are collected around the body (Fig. 1). The 3D activity distribution can be reconstructed from projections.

One of the largest application fields of the SPECT technology is parallel imaging based myocardial perfusion scintigraphy. Any image improvements resulting from the evaluation of the distortions and noise phenomena have significant effect on the diagnostic value of this field. Several distortion effects have been compensated inherently - non-uniform photon absorption and non-liner distant dependent spatial resolution (DDSR) effects of the imaging - by our developed novel 3D iterative reconstruction method (Szlávecz et al. (2010), Szlávecz et al. (2011)). During verification of the algorithm equivocal hypo-perfusion segment has been detected around the apical region of the myocardium systematically on both mathematical phantoms, physical phantoms and in human studies. The phenomenon is well known in myocardial perfusion SPECT studies, and has been investigated by other researchers (Purser et al. (2008) Links et al. (2004)) and is considered as a side effect of attenuation correction. We concluded during the discovery of the problem that the Partial Volume Effect (PVE) phenomenon may cause the distortion. The aim of the current research is to discover the impact of the 3D parallel projection based reconstruction parameters on the apical lesion effect.

2. METHODS

2.1 MLEM based 3D image reconstruction for SPECT imaging

We have created a fast GPU based Maximum Likelihood Expectation Maximization (MLEM) (Shepp and Vardi

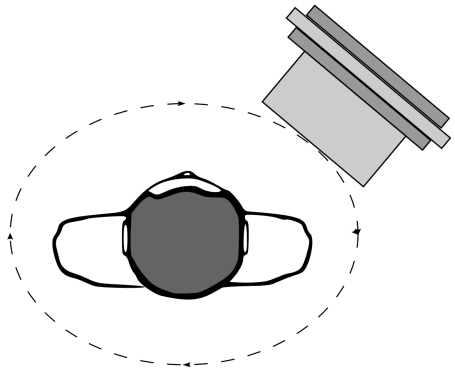

Fig. 1. During SPECT imaging a radionuclide is injected into the body. A gamma camera is rotated around the body and projection images are collected. After data acquisition the 3D distribution of the radioactive substance can be reconstructed using appropriate reconstruction algorithm.

(1982) and Lange and Carson (1984)) reconstruction algorithm for parallel SPECT imaging that compensates for gamma photon attenuation and the distance dependent spatial resolution of the gamma camera (Szlávecz et al. (2010), Szlávecz et al. (2011)).

The developed reconstruction algorithm calculates the activity distribution which has produced the measured values with the highest likelihood according to the following equation:

$$f_j^{k+1} = f_j^k \cdot \frac{1}{\sum_{i=1}^{I} g(j,\theta,s) \otimes \left[a(j,\theta,s) \cdot e^{-\sum_{n\in N_{ij}} c_{in}\cdot\mu_n} \right]} \cdot \cdot \sum_{i=1}^{I} \frac{g(j,\theta,s) \otimes \left[b_i \cdot a(j,\theta,s) \cdot e^{-\sum_{n\in N_{ij}} c_{in}\cdot\mu_n} \right]}{\sum_{n=1}^{J} g(j,\theta,s) \otimes \left[f_n^k \cdot a(n,\theta,s) \cdot e^{-\sum_{h\in N_{in}} c_{ih}\cdot\mu_h} \right]} \quad (1)$$

There is J image voxels, I detector pixels, (θ, s) define a detector pixel location, and $a(j, \theta, s)$ is the probability that a photon emitted in voxel j is detected in detector location (θ, s). In parallel SPECT imaging $a(j, \theta, s)$ is proportional to the crossing length between the image pixel and the perpendicular line toward the detector pixel location.

In equation (1), $g(j, \theta, s)$ represents the distance dependent resolution of the gamma camera:

$$g(j,\theta,s) = \frac{1}{2\cdot\pi\cdot\sigma} \cdot e^{-\frac{s^2}{2\cdot\sigma^2}} \quad (2)$$

$$\sigma = \sqrt{\sigma_{intr}^2 + (psfa + d\cdot psfb)^2} \quad (3)$$

where d is the distance between image voxel j and detector location (Θ, s), $psfa$ and $psfb$ are the parameters of the linear equation and describe the distance dependent resolution of the gamma camera. The function $g(j, \theta, s)$ can be determined with a calibration procedure (Szlávecz et al. (2010), Szlávecz et al. (2011)).

$\mu(x)$ represents the material distribution of the non-homogeneous attenuating medium containing total attenuation coefficients. The total attenuation coefficients represents the attenuation factor caused by all the physical phenomenons, such as photoelectric absorption and Compton scattering, and has been obtained from the XCOM database of National Institute of Standards and Technologies (NIST (2010)). In our realization (a multi-modality SPECT/CT sytem) $\mu(x)$ is derived from a CT scan.

The algorithm itself implements compensation for the gamma photon attenuation, but in this research we investigated the apical phenomenon using only compensation of detector blurring. There was no attenuating medium in the investigated phantoms or configurations.

2.2 Creating Bullseye for myocardial perfusion SPECT imaging

In myocardial perfusion SPECT imaging the result is represented in a polar map, called the "bulls-eye" (see Fig. 2). The bulls-eye is a standard representation of the left ventricular perfusion and is independent of size and orientation of the heart. This representation is investigated by medical doctors for diagnosis purposes to detect ischemic and infarcted regions.

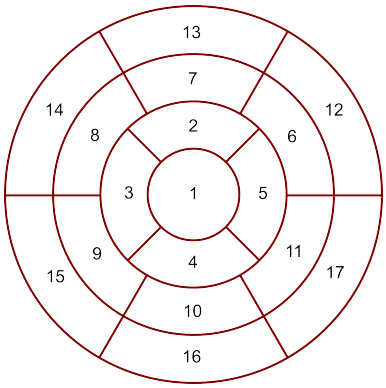

Fig. 2. Regions in the bullseye.

Each pixel value in the bulls-eye is calculated as the maximum value along a line in the reconstructed volume, shown in Fig. 3. The "upper part" of the bullet shaped left ventricular is treated as a spherical model, and line profiles are taken according to the Fig. 3. Similarly, the "lower part" of the ventricular is treated as a ring shaped model.

After the bulls-eye is generated the percentage sums for all regions in Fig. 2 are calculated.

2.3 Investigated cases and phantoms

A mathematical phantom similar to the myocardium structure (bullet phantom), as well as the NCAT phantom which is a mathematical representation of the human thorax, was used in the investigation. The bullet phantom was applied in two orientations. First it was placed upright

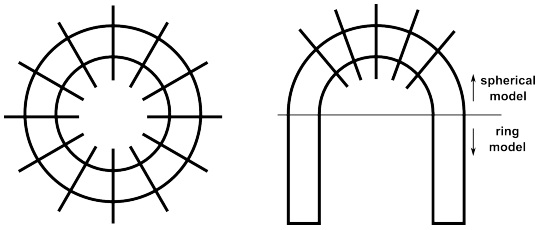

Fig. 3. Each pixel value in the bulls-eye is calculated as the maximum value along a line in the reconstructed volume.

in the center of rotation (Fig. 4(a)), then it was placed off centre rotated 15°, approximately representing an anatomically proper heart location and orientation (Fig. 4(b)).

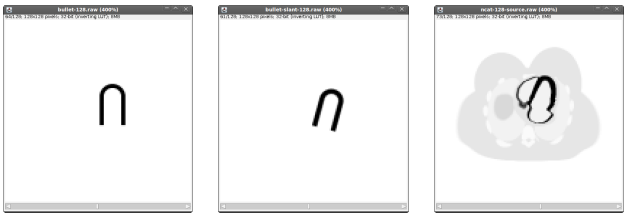

(a) Bullet phantom (b) Slant bullet phantom (c) NCAT phantom

Fig. 4. Phantoms used in the investigation.

Projection images were generated by the forward projection operator of our MLEM based reconstruction algorithm, with attenuation correction and compensation for the DDSR effect. The apical lesion phenomenon has been tested by function of various spatial resolutions and imaging blurring. Two different discretizations of the volume have been applied: 256^3 discretization by voxel sizes of $2mm$; and 128^3 discretization by voxel sizes of $4mm$. The extent of the detector blurring effect was set according to the Mediso Ltd. AnyScan^{TM}SC (multi-modality SPECT/CT) system with a LEHR collimator. The apical lesion effect has been tested as a function of detector blurring extent.

During reconstruction the distance of the actual estimated reconstructed volume to the reference volume has been calculated in each iteration. The convergence curve was in each case monotone decreasing. After 100 iterations there were no significant changes in the convergence curve, so 100 iterations have been performed for all results evaluated in this study.

3. RESULTS AND DISCUSSION

In the first step we have investigated the bullet phantom by applying different extents of detector blurring. Three different extents of blurring have been used in the investigation, listed in Table 1. The extent of the detector blurring effect in case three (psf1) corresponds to the blurring of the Mediso Ltd. AnyScan^{TM}SC (multi-modality SPECT/CT) system with LEHR collimator. In case two (psf0.5) a smaller blurring extent is investigated by halving the distance dependent fraction of blurring, and case one (psf0) represents no blurring at all.

Projection images were generated by the forward projection operator of our MLEM based reconstruction algorithm with compensation for the DDSR effect with detector blurring extents listed in Table 1. In this test case the volume discretization of 128^3 has been applied with voxel size of $4\,mm$

Table 1. Different detector blurring extents used in the investigation.

	σ_{intr}	psfa	psfb
psf0	$0\,mm$	$0\,mm$	0
psf0.5	$4\,mm$	$1\,mm$	0.00175
psf1	$4\,mm$	$1\,mm$	0.035

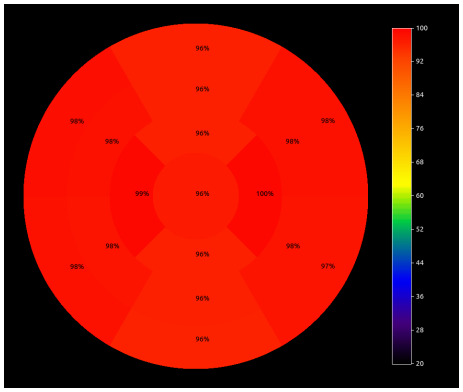

(a) psf0

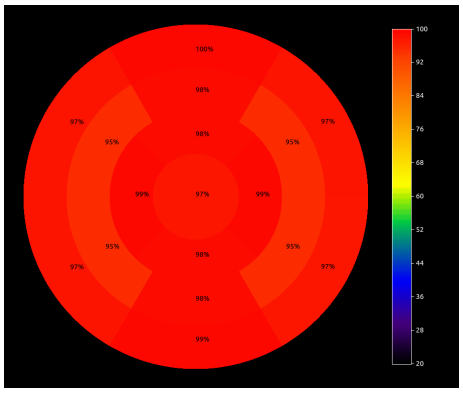

(b) psf0.5

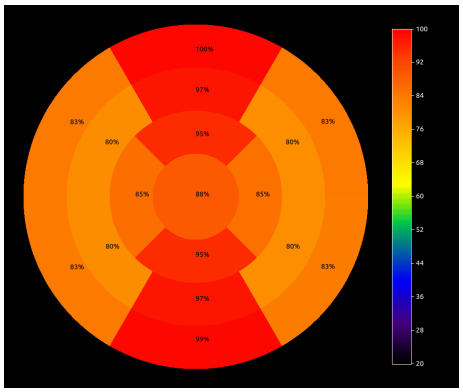

(c) psf1

Fig. 5. Bulls-eyes of bullet phantoms while investigating the effect of detector blurring extent. The values in the apex are listed in Table 2.

The bulls-eyes generated from the three reconstructions are shown in Fig. 5, and the apex values are listed in Table 2. The apex values suggest a relationship between

Table 2. Effect of different detector blurring extents listed in Table 1. to the apex.

Case	pas0	paf0.5	psf1
Apex value	96%	97%	88%

Table 3. Effect of phantom location and orientation to the apex. For comparison the apex values of straight bullet are also listed in the table.

Case	psf0	psf0.5	psf1
Bullet Apex value	96%	97%	88%
Slant bullet apex value	96%	98%	90%

Table 4. Effect of different detector blurring extents listed in Table 1. to the apex in case of the NCAT phantom.

Case	psf0	psf0.5	psf1
Apex value	98%	90%	82%

the blurring extent and the decreased activity around apical region. Increased blurring extent results in lower apical activity. However, the growth is not linear. The half blurring extent (psf0.5) performed slightly worse whet its bulls-eye was compared to the no blurring case (psf0), but the apical region is not significantly affected.

In the second step we have tried to evaluate relationship between the apical phenomenon and the location and orientation of the bullet shaped phantom. Thus we slanted the bullet phantom and moved a bit off center (see Fig. 4(b)) in order to generate a phantom with a shape, location and orientation of an anatomically correct heart. The slant bullet phantom was also investigated with the three blurring extents listed in Table 1.

In this case projection images were also generated by the forward projection operator of our MLEM based reconstruction algorithm, with compensation for the DDSR effect with detector blurring extents listed in Table 1. The volume discretization of 128^3 has been applied with voxel size of $4\,mm$. Similar to the first case, the three different blurring extents (listed in Table 1.) were investigated.

Bulls-eyes generated from reconstructed slant bullet phantoms are shown in Fig. 6. Apex values are listed in Table 3. Results in Table 3 indicate that changes in location and orientation does not result in a significance difference in the investigated apical phenomenon. Approximately the same apical failure is visible in both cases.

In the third step we have utilised the NCAT phantom (Segars et al. (1999)) that is a real mathematical representation of the human thorax. Similarly to the phantoms above, projection images were generated by the forward projection operator of our MLEM based reconstruction algorithm with compensation for the DDSR effect with detector blurring sizes listed in Table 1. The volume discretization of 128^3 has been applied with voxel size of $4\,mm$.

Fig. 7 shows the bulls-eyes generated from the reconstructed images and the measured apex values are listed in Table 4. Similar to the bullet phantoms, increased detector blurring extent caused more serious apical lesion when

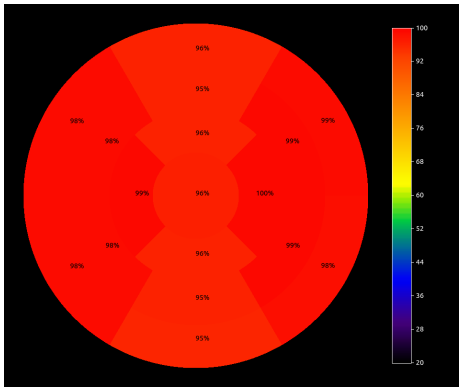

(a) psf0

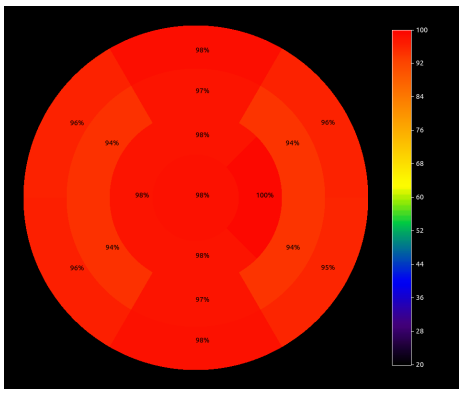

(b) psf0.5

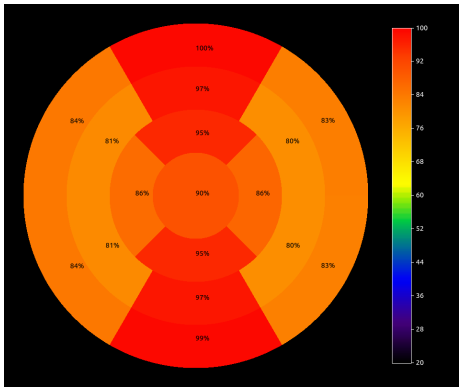

(c) psf1

Fig. 6. Bulls-eyes of bullet phantoms while investigating the effect of location and orientation. The values in the apex are listed in Table 3.

the NCAT phantom was utilised. However, activity in the NCAT phantom apex is significantly lower also if half blurring is applied (psf0.5).

An assumed relationship between the orientation of heart shaped phantoms and apical lesion indicated that the slanted bullet phantom should be applied. The orientation of the slanted bullet corresponds approximately to the orientation of the heart in case of myocardial perfusion studies. However, the results derived from the reconstruction of slanted bullet seem not to support this assumption. The bullet and slant bullet phantom cases resulted in similar outcome: there was no significant difference in apical region. Additionally, the half blurring case resulted in a significantly better bulls-eye compared to the NCAT

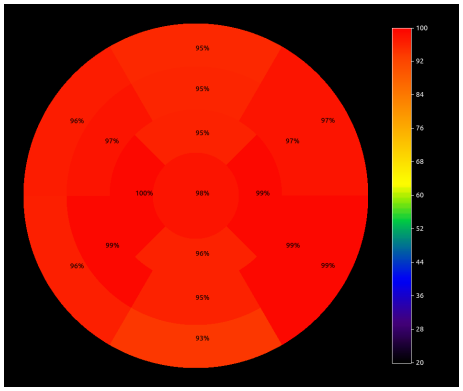

(a) psf0

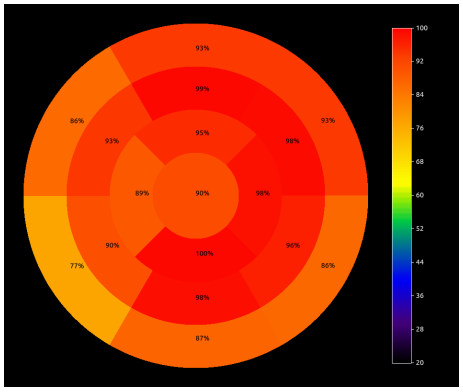

(b) psf0.5

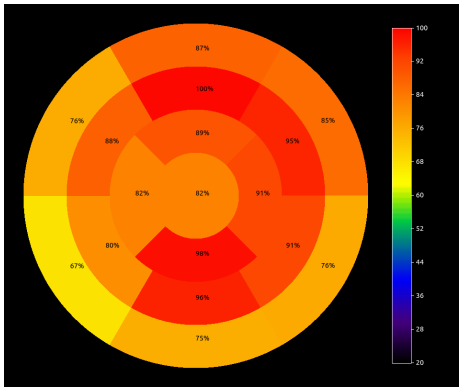

(c) psf1

Fig. 7. Bulls-eyes of NCAT phantom with different extent of detector blurring. The values in the apex are listed in Table 4.

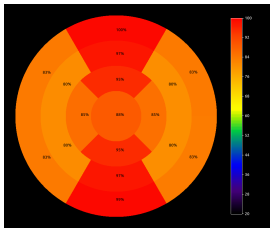

(a) Bullet 128

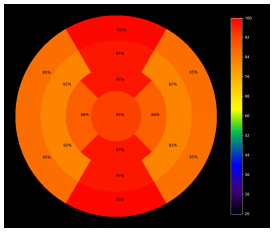

(b) Bullet 256

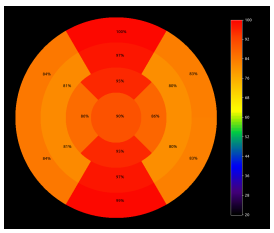

(c) Slant bullet 128

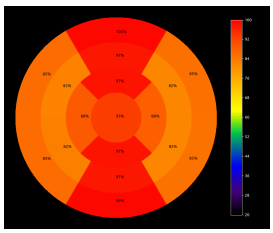

(d) Slant bullet 256

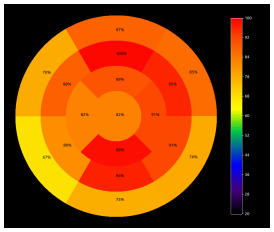

(e) NCAT 128

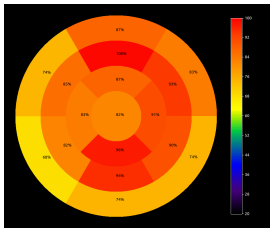

(f) NCAT 256

Fig. 8. Generated bulls-eyes of reconstructed volumes with different discretizations.

Table 5. Effect of different discretization (e.g. better spatial resolution). Extent of detectro blurring: $\sigma_{intr} = 4mm$, $psfa = 1mm$, $psfb = 0.035$.

	128	256
Bullet Apex value	88%	93%
Slant bullet apex value	90%	93%
NCAT apex value	82%	82%

phantom. In spite of the fact that the apical phenomenon seems not to depend on the orientation of the phantom we will continue to investigate this assumption as sometimes individual result were contradictory. Investigations are planned with the slant bullet phantom at several angles between 0 and 2π.

Theoretically, lower apical defect can be achieved with a better reconstruction, resulting in better spatial resolution. In the last step of this study we investigated the influence of spatial resolution on the apical lesion phenomenon. The bullet, slant bullet and NCAT phantoms were investigated in a higher volume discretization: 256^3 volume by voxel sizes of $2mm$. Results can be found in Fig. 8 and in Table 5.

In the case of bullet and slant bullet phantom there is a slight improvement ($\sim 90\% \rightarrow \sim 93\%$) but the improved spatial resolution seem not to affect the apical region in the case of the NCAT phantom.

4. CONCLUSION

In myocardial perfusion SPECT imaging equivocal hypoperfusion segment have been detected around the apical region of the myocardium systematically on both mathematical phantoms, physical phantoms and in human studies. We concluded that the Partial Volume Effect (PVE) phenomenon may result in the distortion. In this work we investigated the impact of the 3D parallel projection based reconstruction parameters on the apical lesion effect. Several reconstruction setups with different parameter settings are executed using different mathematical phantoms modelling the myocardium.

The apical lesion effect has been tested as a function of detector blurring extent. Increased detector blurring extent caused more serious apical lesion.

Results of this study indicates that the apical lesion effect does not depend on the location and orientation of the activity distribution.

The degree of apical lesion has been decreased if 256^3 volume with voxel sizes of $2mm$ were applied instead of the 128^3 volume with voxel sizes of $4mm$. Higher resolution volume reduced Partial Volume Effect. Smaller extent of detector blurring resulted less apical lesion, as well.

As the subsequent step of the research we are going to investigat the relationship between the orientation of the heart and the apical lesion. Additionally, we will analyze the influences of some distortion effects, such as gamma photon attenuation and Compton scattering, around the apical segment of the myocardium.

ACKNOWLEDGEMENTS

This work was supported by Mediso Ltd. and by the Hungarian National Research Found (OTKA) Grants No. CK80316 and K82066.

REFERENCES

Lange, K. and Carson, R. (1984). EM reconstruction algorithms for emission and transmission tomography. *Journal of Computer Assisted Tomography*, 8(2), 306–316.

Links, J., Becker, L., and Anstett, F. (2004). Clinical significance of apical thinning after attenuation correction. *Journal of nuclear cardiology : official publication of the American Society of Nuclear Cardiology*, 11(1), 26 – 31.

Miles N. Wernick, J.N.A. (2005). *Emission Tomography: The fundamentals of SPECT and PET*. Springer-Verlag London.

NIST (2010). Xcom: Photon cross sections database. `http://www.nist.gov/index.html`.

Purser, N.J., Armstrong, I.S., Williams, H.A., Tonge, C.M., and Lawson, R.S. (2008). Apical thinning: real or artefact? *Nuclear Medicine Communications*, 29(4), 382 – 506. doi:10.1097/MNM.0b013e3282f4a22e.

Segars, W., Lalush, D., and Tsui, B. (1999). A realistic spline-based dynamic heart phantom. *Nuclear Science, IEEE Transactions on*, 46(3), 503 –506.

Shepp, L.A. and Vardi, Y. (1982). Maximum likelihood reconstruction for emission tomography. *Medical Imaging, IEEE Transactions on*, 1(2), 113 –122.

Szlávecz, A., Hesz, G., Puskás, Z., Kári, B., Pártos, O., Györke, T., Bükki, T., Domonkos, B., and Benyó, B. (2010). A Fast Iterative GPU-based Reconstruction Algorithm for SPECT Imaging Involving Collimator and Attenuation Compensation. *European Journal of Nuclear Medicine and Molecular Imaging*, 37(Supplement 2), S284 – S284.

Szlávecz, A., Hesz, G., Bükki, T., Kári, B., and Benyó, B. (2011). GPU-Based Acceleration of the MLEM Algorithm for SPECT Parallel Imaging with Attenuation Correction and Compensation for Detector Response. In *Proceedings of the 18th IFAC World Congress. Milan, Italy.*, 6195–6200. doi:10.3182/20110828-6-IT-1002.02896.